ACS OMEGA

http://pubs.acs.org/journal/acsodf

Article

Novel Pyrano[3,2-*c*]quinoline-1,2,3-triazole Hybrids as Potential Anti-Diabetic Agents: *In Vitro* α-Glucosidase Inhibition, Kinetic, and Molecular Dynamics Simulation

Soheila Esmaili, Ahmad Ebadi, Ardeshir Khazaei, Hamideh Ghorbani, Mohammad Ali Faramarzi, Somayeh Mojtabavi, Mohammad Mahdavi, and Zahra Najafi*

Cite This: *ACS Omega* 2023, 8, 23412−23424

Read Online

ACCESS | Metrics & More | Article Recommendations | Supporting Information

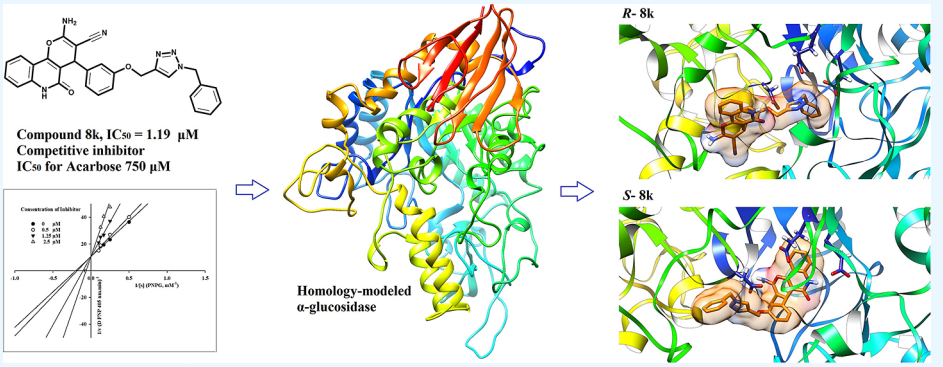

ABSTRACT: In this study, a novel series of pyrano[3,2-*c*]quinoline-1,2,3-triazole hybrids **8a−o** were synthesized and evaluated against the α-glucosidase enzyme. All compounds showed significant in vitro inhibitory activity (IC_{50} values of 1.19 ± 0.05 to 20.01 ± 0.02 μM) compared to the standard drug acarbose (IC_{50} = 750.0 μM). Among them, 2-amino-4-(3-((1-benzyl-1*H*-1,2,3-triazol-4-yl)methoxy)phenyl)-5-oxo-5,6-dihydro-4*H*-pyrano[3,2-*c*]quinoline-3-carbonitrile (compound **8k**) demonstrated the best inhibitory effect toward α-glucosidase (IC_{50} = 1.19 ± 0.05 μM) with a competitive pattern of inhibition. Since compound **8k** was synthesized as a racemic mixture, molecular docking and dynamics simulations were performed on *R*- and *S*-enantiomers of compound **8k**. Based on the molecular docking results, both *R*- and *S*-enantiomers of compound **8k** displayed significant interactions with key residues including catalytic triad (Asp214, Glu276, and Asp349) in the enzyme active site. However, an in silico study indicated that *S*- and *R*-enantiomers were inversely located in the enzyme active site. The *R*-enantiomer formed a more stable complex with a higher binding affinity to the active site of α-glucosidase than that of the *S*- enantiomer. The benzyl ring in the most stable complex ((*R*)-compound **8k**) was located in the bottom of the binding site and interacted with the enzyme active site, while the pyrano[3,2-*c*]quinoline moiety occupied the high solvent accessible entrance of the active site. Thus, the synthesized pyrano[3,2-*c*]quinoline-1,2,3-triazole hybrids seem to be promising scaffolds for the development of novel α-glucosidase inhibitors.

1. INTRODUCTION

Diabetes mellitus (DM) is a chronic disease caused by an inherited or acquired defect in insulin secretion or a decrease in response of organs to secreted insulin.[1] The bodies of people with DM do not produce enough insulin, which is responsible for lowering blood sugar levels.[2] If diabetics are not treated, their blood glucose levels may increase significantly,[3,4] and this may lead to kidney failure, cardiovascular disease, blindness, and impaired wound healing. α-Glucosidase (EC 3.2.1.20) is a carbohydrate-hydrolyzing enzyme, and its catalytic activity, as an intestinal digestive enzyme, results in cleavage of poly- and disaccharides into monosaccharides (glucose), which in turn will raise blood sugar levels.[5,6] Therefore, several α-glucosidase inhibitors (AGIs) such as acarbose,[7] voglibose,[8] miglitol,[9] and nojirimycin[10] are widely used alone or in combination with insulin injection as treatment of diabetes. However, these drugs are often non-specific agents that may cause certain side effects such as indigestion, bloating, and diarrhoea.[11] Although there are common medications to control diabetes, many challenges are encountered in the effective treatment of diabetes, including optimizing common treatments to regulate glucose concentration while reducing side effects. In the recent years, the

Received: January 8, 2023
Accepted: May 30, 2023
Published: June 20, 2023

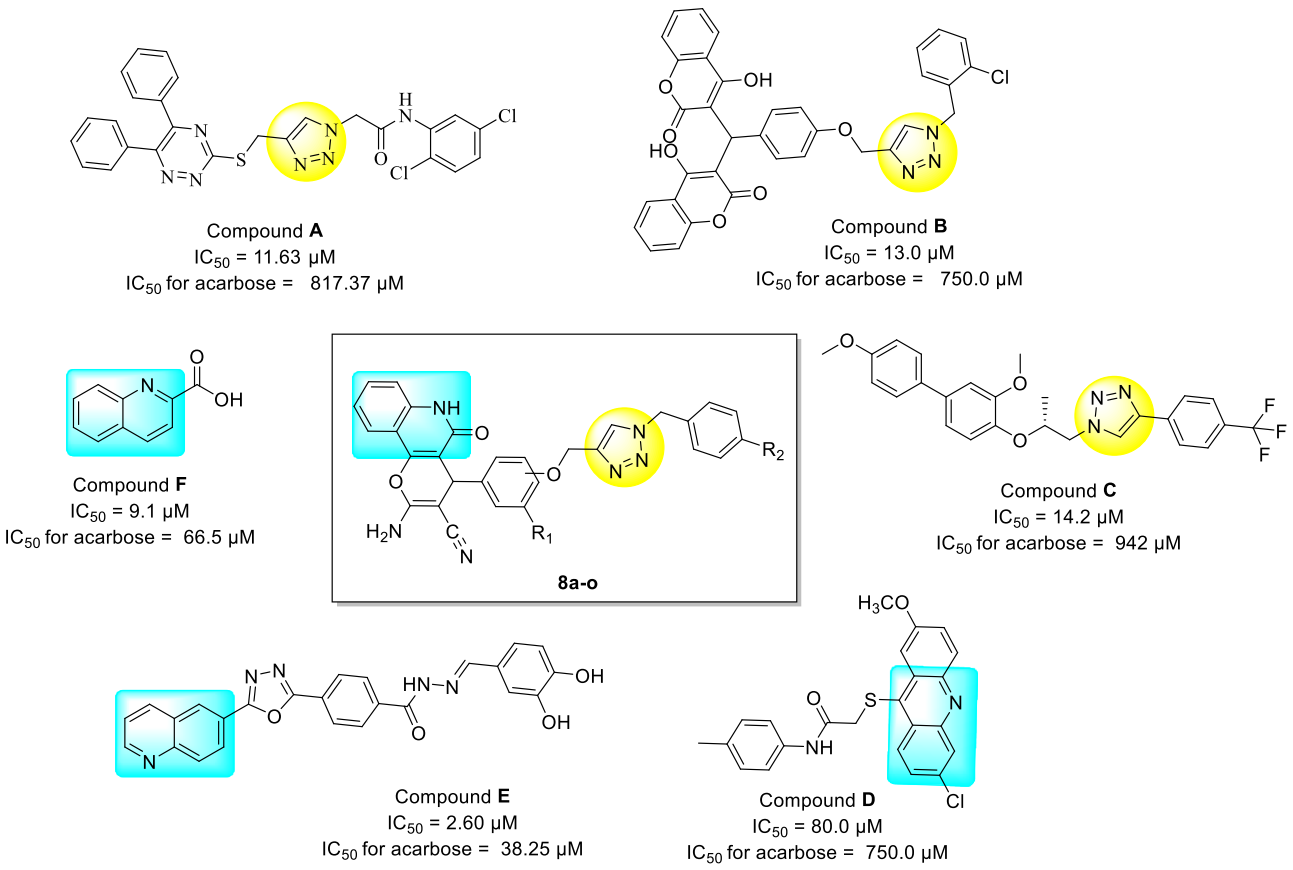

Figure 1. Designed pyrano[3,2-*c*]quinoline −1,2,3-triazole hybrids based on 1,2,3-triazole and quinoline scaffolds.

management and control of diabetes using AGIs have received much attention from pharmacists.[12,13]

N-heterocyclic compounds especially those with triazole rings such as 1,2,3-triazole have different biological properties such as anti-Alzheimer,[14,15] anti-viral,[16,17] anti-fungal,[18] anti-bacterial and antitubercular,[19] anti-cancer,[20] anti-tubulin,[21−24] and anti-diabetes[25−30] activity. Till date, many scaffolds containing 1,2,3-triaole rings with significant inhibitory activity against α-glucosidase have been reported (some of them are depicted in Figure 1, compounds **A**, **B**, and **C**[25−27]). Besides, quinoline- and quinoline-fused derivatives (Figure 1 compounds **D**, **E**, and **F**) have successfully been applied by medicinal chemists as effective pharmacophores in designing of new α-glucosidase inhibitors.[28−30] Based on the above-mentioned points and in continuation of our interest in synthesis of novel bioactive agents,[31,32] herein, we reported synthesis of a novel series of quinoline-1,2,3-triazole hybrids **8a−o** as α-glucosidase inhibitors. These compounds were synthesized via the Cu-catalyzed azide−alkyne cycloaddition method (click chemistry) to produce a 1,2,3-triazole linkage. *In vitro* evaluation, kinetic, molecular docking, and dynamics studies against α-glucosidase were performed to understand their therapeutic potentials for the treatment of type 2 DM.

2. RESULTS AND DISCUSSION

2.1. Chemistry. To synthesize products **8a−o**, several steps were performed according to Scheme 1. In the first step, propargylated aldehydes **3a−c** were obtained by a reaction between aldehydes **1a−c** and propargyl bromide in dimethyl formamide (DMF) at ambient temperature for 24 h.[33] In the second step, compounds **6a−c** were synthesized by multi-component reaction between malononitrile, 4-hydroxyquinolin-2(1*H*)-one, and compounds **3a−c** in the presence of a catalytic amount of ammonium acetate in ethanol solvent. In the third step, benzyl bromide derivatives **7a−c** were converted to benzyl azide derivatives in DMF and reacted with compounds **6a−c** to obtain desired compounds **8a−o** in the presence of Et_3N, ascorbic acid, and $CuSO_4{\cdot}5H_2O$ in DMF/H_2O (4:1) at room temperature.[14,15] After completion of the reaction, ice was added to the reaction mixture and the resulting precipitates of compounds **8a−o** were filtered and washed with water. The structures of all synthesized compounds were confirmed using ^{1}H NMR,^{13}C NMR, mass spectroscopy, and elemental analyses.

2.2. Biological Study. *2.2.1. In Vitro α-Glucosidase Inhibitory Activity.* The synthesized compounds **8a−o** were evaluated for their *in vitro* inhibitory activity against α-glucosidase and compared to the standard inhibitor acarbose. The obtained results were expressed as mean ± S.E. of three independent experiments in the Table 1. All the synthesized compounds showed significant inhibition against α-glucosidase with an IC_{50} value of 1.19 ± 0.05 to 23.2 ± 0.8 μM in comparison to acarbose, as a reference drug with an IC_{50} of 750.0 ± 1.5.

Based on the aryloxy phenyl linker between pyrano[3,2-*c*]quinoline scaffold and benzyl-1,2,3-triazole pendant group, the synthesized compounds **8a−o** can be divided into three series: (1) compounds **8a−e** with a 4-aryloxy phenyl linker, (2) compounds **8f−j** with a 3-methoxy 4-aryloxy phenyl linker, and (3) compounds **8k−o** with a 3-aryloxy phenyl linker. Among the synthesized compounds, compound **8k** of the third series with un-substituted benzyl moiety showed the best

https://doi.org/10.1021/acsomega.3c00133
ACS Omega 2023, 8, 23412−23424

Scheme 1. Synthesis of Pyrano[3,2-*c*]quinoline-1,2,3-triazole Hybrids 8a−o

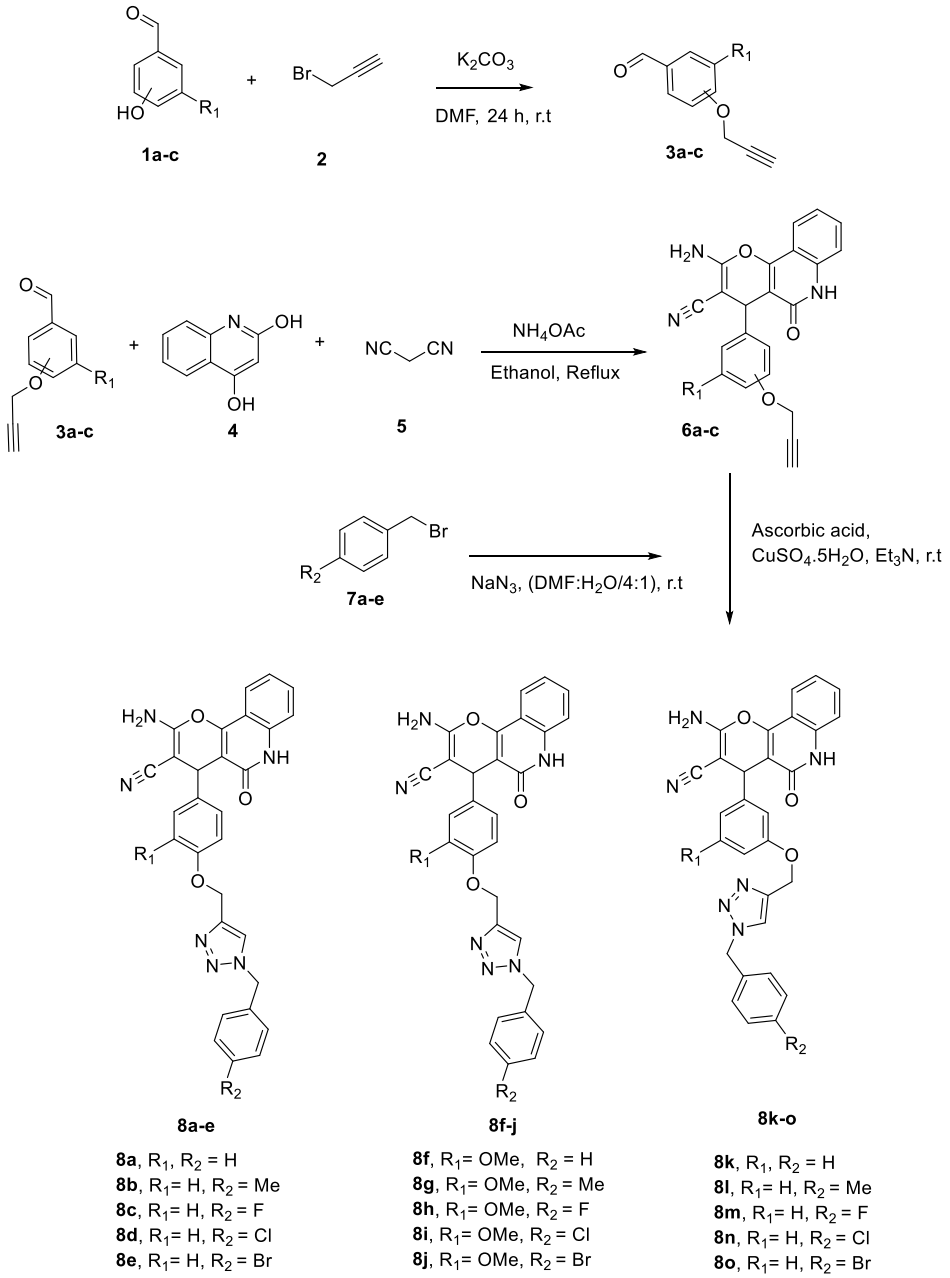

inhibitory activity (IC_{50} = 1.19 ± 0.05 μM). To evaluate the structure−activity relationships (SARs) for α-glucosidase inhibitory activity, substitution of the hydrogen atom with other chemical groups was carried out at the 4th position of the pendant benzyl moiety.

The IC_{50} value of the unsubstituted compound **8a** was 20.01 ± 0.02 μM. The introduction of methyl, fluoro, chloro, and bromo substituents at the 4th position of the pendant benzyl group led to produce compounds **8b**, **8c**, **8d**, and **8f** with IC_{50} values of 9.72 ± 0.18, 12.06 ± 0.03, 14.67 ± 0.06, and 4.48 ± 0.03 μM, respectively. As presented in Table 1, the replacement of the hydrogen atom with the methyl group, as a hydrophobic electron donating group (EDG), at the 4th position of the benzyl moiety in compound **8b** increased its inhibitory activity by twofold. Furthermore, introduction of the electron-withdrawing groups (EWGs) in the benzyl moiety increased inhibitory activity in the following order 4-Br > 4-F > 4-Cl in compounds **8f**, **8c**, and **8d** with IC_{50} values of 4.48 ± 0.03, 12.06 ± 0.03, and 14.67 ± 0.06 μM, respectively. It seems that the polarizability with the atomic size of substituents on the *n*-benzyl pendant moiety affected inhibitory activity more than that of the electronic effect. Therefore, bromine with the largest size exhibited better inhibitory activity than fluorine and chlorine.

In the second series, compounds **8f−j** had a 3-methoxy-4-aryloxy phenyl linker. Compound **8f** with an unsubstituted benzyl moiety exhibited an inhibitory activity (IC_{50} of 23.2 ± 0.8 μM) similar to compound **8a** of the first series (IC_{50} = 20.01 ± 0.02 μM). Compound **8g** with the 4-methyl group at the pendant benzyl moiety exhibited better inhibitory activity (IC_{50} = 9.9 ± 0.5 μM) compared to compound **8f**. Introduction of the EWGs including 4-F, 4-Cl, and 4-Br led to enhanced inhibitory activity in the compounds **8h**, **8i**, and **8j** with IC_{50} values of 15.9 ± 0.2, 9.0 ± 0.5, and 14.0 ± 0.7 μM,

https://doi.org/10.1021/acsomega.3c00133
ACS Omega 2023, 8, 23412−23424

Table 1. Inhibitory Activities of the New Compounds 8a−o Against α-glucosidase[a]

entry	compound	R_1	R_2	IC_{50} (μM) ± SE[a]
1	**8a**	H	H	20.01 ± 0.02
2	**8b**	H	4-Me	9.72 ± 0.18
3	**8c**	H	4-F	12.06 ± 0.03
4	**8d**	H	4-Cl	14.67 ± 0.06
5	**8e**	H	4-Br	4.48 ± 0.03
6	**8f**	OMe	H	23.2 ± 0.8
7	**8g**	OMe	4-Me	9.09 ± 0.5
8	**8h**	OMe	4-F	15.9 ± 0.2
9	**8i**	OMe	4-Cl	9.9 ± 0.5
10	**8j**	OMe	4-Br	14.0 ± 0.7
11	**8k**	H	H	1.19 ± 0.05
12	**8l**	H	4-Me	14.52 ± 0.05
13	**8m**	H	4-F	8.87 ± 0.03
14	**8n**	H	4-Cl	15.13 ± 0.15
15	**8o**	H	4-Br	9.19 ± 0.17
acarbose				750 ± 1.5

[a]Values are the mean ± standard error of the mean. All experiments were performed at least three times.

respectively. Also, compound **8g** with 4-methyl substitution showed an inhibitory activity (IC_{50} = 9.09 ± 0.5 μM) similar to compound **8i** with 4-chlorine substitution, indicating that both electron-donating (Me) and electron-withdrawing (Cl) effects along with lipophilicity were likely important in the inhibitory activity level. In this series, the inhibitory activities were probably affected by the 3-methoxy group at the linker phenyl ring due to the strict effect and perpendicular conformational to benzyl-1,2,3-triazole and pyrano[3,2-c]quinoline moieties.

In the third series, compounds **8f−j** had a 3-aryloxy-phenyl linker. The presence of aryloxy at 3rd position of the phenyl ring could change the conformation of the pendant benzyl-1,2,3-triazole moiety to the linker and another part of the structure. Compound **8k** with un-substituted benzyl moiety exhibited the best inhibitory activity (IC_{50} = 1.19 ± 0.05 μM). Introduction of the methyl group, as the EDG, at the 4th position of the benzyl moiety produced compound **8l** and led to decreased inhibitory activity (IC_{50} = 14.52 ± 0.05) in comparison to compound **8k**. Compounds **8m**, **8n**, and **8o** with EDGs including 4-F, 4-Cl, and 4-Br also exhibited decreased inhibitory activity with IC_{50} values of 8.87, 15.13, and 9.19 μM, respectively. The obtained results revealed that the electron-withdrawing effect of fluorine and the polarizability with the atomic size of bromine in the pendant phenyl group were more critical than lipophilicity.

In general, it is evident from the results that changing the position of the aryloxy-phenyl from 4th-to 3rd position increased the inhibitory activity against α-glucosidase enzyme.

2.2.2. Kinetic Study. The kinetic study of the most active compound **8k** against α-glucosidase was performed in order to determine inhibition mode of the synthesized compound. As shown in Figure 2a, the Lineweaver−Burk plot indicated that with increasing concentrations of compound **8k**, the K_m gradually increased, while V_{max} remained unchanged. This finding demonstrated that compound **8k** was a competitive inhibitor toward the α-glucosidase enzyme. Furthermore, the plot of the K_m versus different concentrations of inhibitor **8k** gave an estimate of the inhibition constant (K_i) with the value of 1.3 μM (Figure 2b).

2.2.3. Homology Modeling. Since the crystal structure of the eukaryotic yeast *Saccharomyces cerevisiae* α-glucosidase is not yet available, homology modeling was used to predict the 3D structure of α-glucosidase. The sequence of *S. cerevisiae* α-glucosidase is made up of 584 amino acid residues. The NCBI's BLAST server suggested isomaltase from baker's yeast as a suitable template for homology modelling. The result of α-glucosidase and isomaltase homology modeling revealed a sequence identity of 72.1%. The quality of the template crystallographic structure was acceptable as 88.9% of residues were located in the favored regions (A, B, and L regions) and 99.8% of residues were placed in the allowed regions (a, b, l, and p regions). The obtained alignment is provided in Figure 3. BLAST results of α-glucosidase and isomaltase showed a score of 909 and an *E* value of zero (0.0). High-scoring models were selected according to the lowest value of the discrete optimized protein energy (DOPE). The overlay of the homology model of α-glucosidase and isomaltase (3A47) showed a perfect match, especially when considering the backbone atoms (Figure 3). We assessed the quality of the

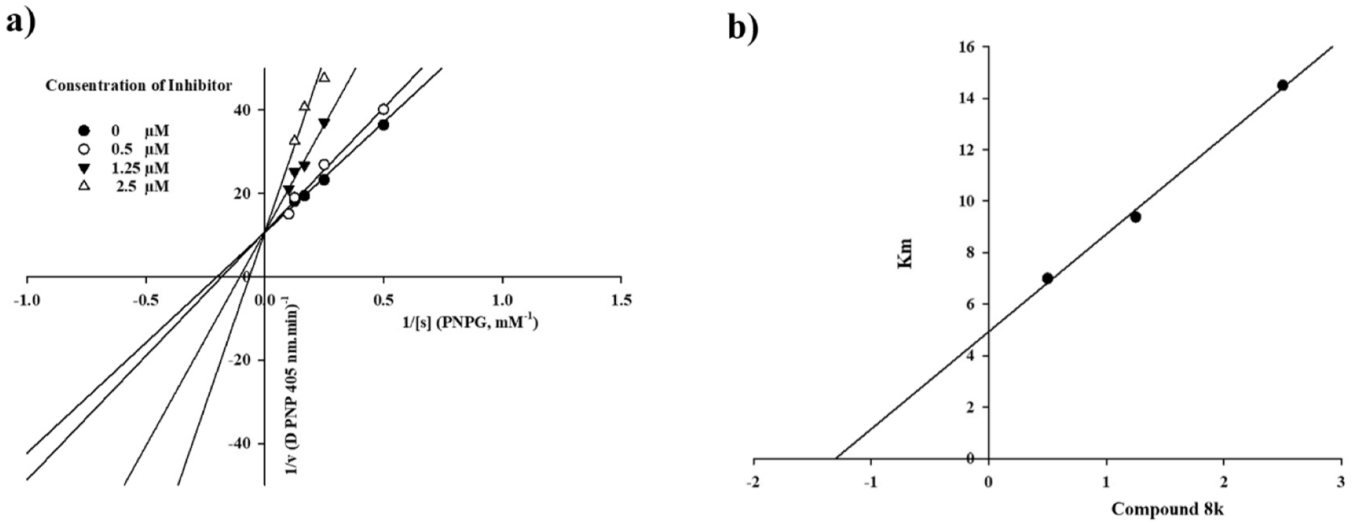

Figure 2. Kinetic study of compound **8k** against the α-glucosidase enzyme. (a) Lineweaver−Burk plot in the absence and presence of different concentrations of compound **8k**; (b) secondary plot between K_m and various concentrations of compound **8k**.

https://doi.org/10.1021/acsomega.3c00133
ACS Omega 2023, 8, 23412−23424

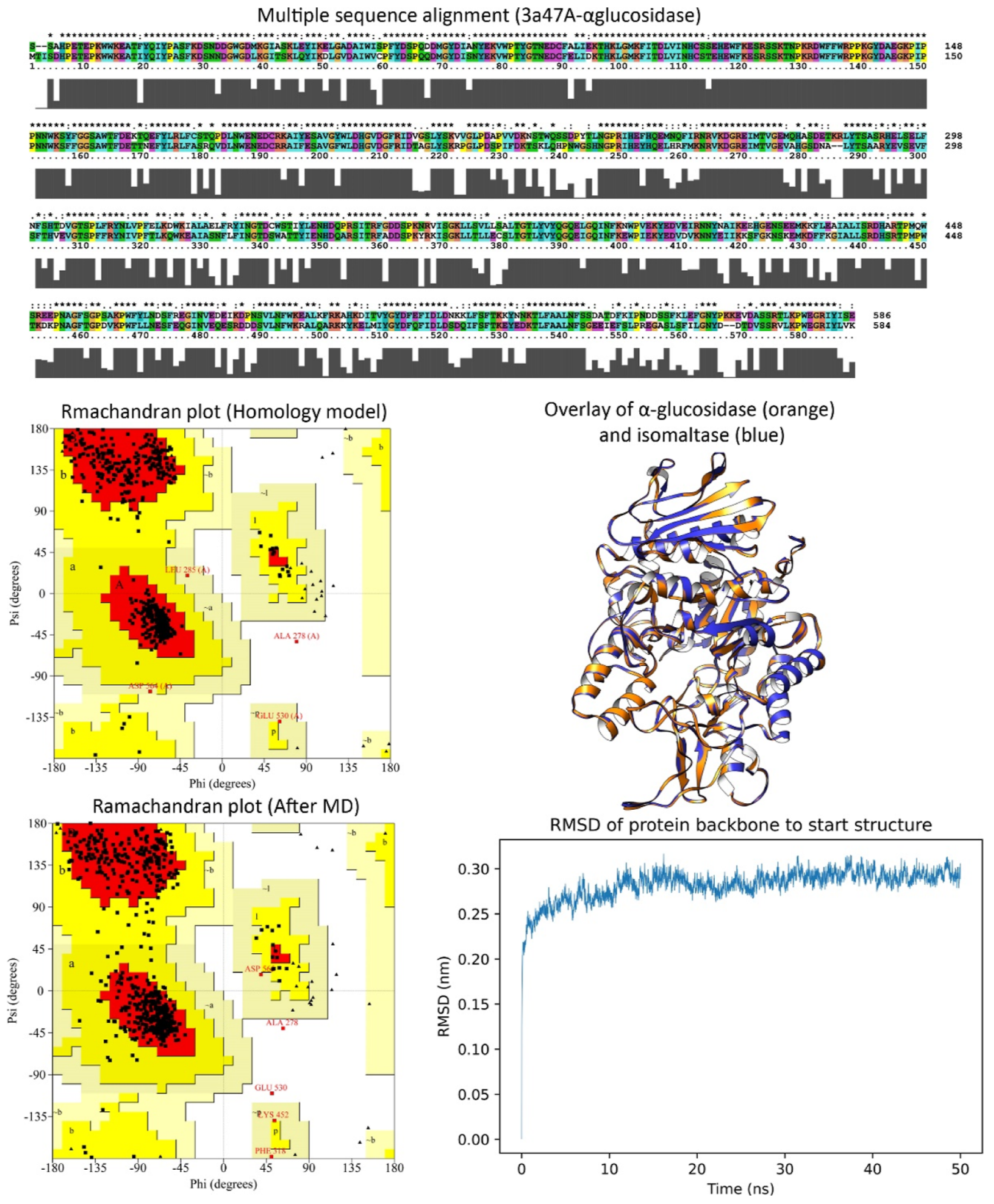

Figure 3. Sequence alignment of the α-glucosidase (P53341) and isomaltase (P53051) enzymes. Ramachandran plots of the homology model and the final model obtained from the MD simulation showed minor differences. Overlaid structure of the homology model and isomaltase indicated a perfect match when considering backbone atoms (rmsd = 1.9 Å). rmsd of the backbone during the MD simulation illustrated that the target protein reached a steady state indicating that isomaltase was a good template for homology modeling of the α-glucosidase enzyme.

selected models by energetically evaluating the allowed regions of the backbone dihedral angles ψ against φ of amino acid residues in the α-glucosidase structure using the Ramachandran plot (Figure 3). In the final model, 93.2% of residues were located in the favored regions (A, B, and L regions) and 99.8% of residues were placed in the allowed regions (a, b, l, and p

https://doi.org/10.1021/acsomega.3c00133
ACS Omega 2023, 8, 23412−23424

regions) as well. The overall quality factor calculated by ERRAT was 86.5%. It should be noted that the ERRAT quality factor, reported for high-resolution structures, is generally around 90% or higher. According to the obtained results, the distribution of distances and angles between the aligned residues in the template and the target protein was comparable.

In this regard, the MODELLER imposed high spatial restraint on the predicted model. To refine the predicted homology model, 50 ns MD simulation was carried out to relax the α-glucosidase structure. Simulation of this enzyme in explicit water revealed minor differences in the backbone dihedral angle values (Figure 3). Backbone rmsd variation of α-glucosidase (0.28 ± 0.017 − rsd <6.03%) (Figure 3) implied that the predicted homology model of α-glucosidase was not affected by the simulation environment dramatically and isomaltase could be a good template for homology modeling of α-glucosidase as well. The dihedral angles ψ against φ of amino acid residues in the α-glucosidase structure were not affected drastically during the MD simulation (99.8 and 99.6% of residues were in the allowed regions before and after the MD simulation). However, the overall 3D quality of the model was modified after the MD simulation and the ERRAT score increased from 86.5%, in the homology model, to 88.9% after the MD simulation.

2.2.4. Molecular Docking Study. To identify possible binding modes of the synthesized compounds in the active site of the α-glucosidase enzyme, a molecular docking study was conducted using AutoDock Tools (version 4.2) on the active site of the modeled α-glucosidase enzyme. To obtain a reliable model for the ligand−enzyme complex, ensemble docking was applied to consider the conformational changes of the enzyme. The trajectories of the α-glucosidase enzyme during the 50 ns MD simulation were clustered into 6 conformers using a 2 Å rmsd cut-off. Acarbose and the selected compounds **8e**, **8g**, and **8k** were docked into the active site of 6 conformers of α-glucosidase.

Based on the literature, the catalytic triad in α-glucosidase is composed of Asp214, Glu276, and Asp349 residues, respectively,[33] and Asp68, Tyr71, Thr215, Asn241, Phe300, Glu304, Ser308, Pro309, Phe311, His348, Arg439, and His111 residues are also key residues in the enzyme active site.[34] Initially, the molecular modeling of the standard inhibitor acarbose was performed to validate the α-glucosidase homology model and docking method. Figure 4 presents the binding mode of acarbose in the active site of the α-glucosidase enzyme. As seen, hydroxyl and amine groups of cyclohexenylamine, as the most important pharmacophoric points of acarbose, formed hydrogen bonds with the catalytic triad (Asp214, Glu276, and Arg439), Tyr71, His348, and Asp68 (Figure 4).[31]

The synthesized compounds possessed one chiral center and were produced as a racemic mixture during synthesis. For a comprehensive in silico study, both enantiomers (R and S) were evaluated in a molecular modeling study. The final intermolecular energy (ΔH), torsional free energy ($\sim -T\Delta S$), estimated free energy of binding (ΔG_b), sum of the square of Mulliken charges ($\sum q^2$), dipole moment (μ), and quadrupole moment (Q) for acarbose and the three potent compounds **8e**, **8g**, and **8k** are given in Table 2. In the case of acarbose, 95% confidence interval (CI) of predicted ΔG_bs in the highest ranked cluster had a wide range after 10^6 cycles of bootstrapping (3.84 kcal/mol). Even in the limited conformational space of the highest ranked cluster, acarbose experienced

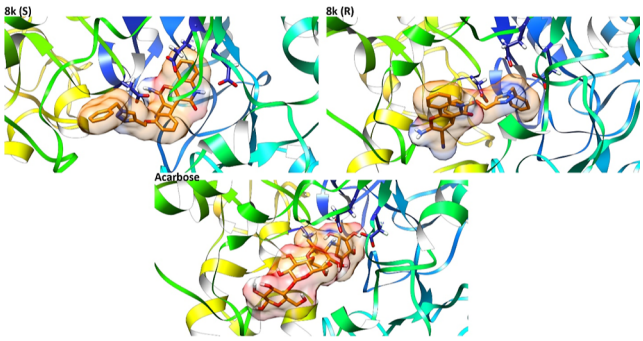

Figure 4. Predicted binding pose of both enantiomers of the compound **8k** and acarbose in the active site of the α-glucosidase enzyme. The catalytic triad residues (Asp214, Glu276, and Asp349) are shown by blue sticks. Ligands are represented by orange sticks. As a type I α-glucosidase inhibitor, acarbose formed hydrogen bond via the NH moiety with Glu276. The docking result indicated that the predicted model met the key interactions proposed in the mechanism of action of the enzyme.

a big gap between the minimum (−10.15 kcal/mol) and the maximum (−7.31 kcal/mol) ΔG_b. The flexibility of acarbose widened the ΔG_b by small conformational changes (rmsd 0−1.98 Å in the highest ranked cluster) that led to less favorable binding mode. Considering 95% CI of the estimated free energy of binding, the difference between affinity of R- and S-enantiomers toward the active site of α-glucosidase was insignificant. So, the docking algorithm could not discriminate between the two enantiomers considering ΔG_b. Considering the ΔH and ΔG_b values, the docking process was successful in predicting the most potent compound (Table 1). However, the 95% CI showed no significant differences between acarbose and the designed compounds **8e**, **8g**, and **8k**. The charge density ($\sum q^2$) could represent the contribution of electrostatic interactions in binding energy. The charge density of the potent compounds was higher than that of the weak ones (acarbose > **8k** > **8g** > **8e**). On the other hand, the same pattern was seen for the quadrupole moments (acarbose > **8g** ∼ **8k** > **8e**). The results indicated that the electrostatic and vdW interactions had a similar importance in the binding process.

Figure 4 depicts the binding mode of both enantiomers of compound **8k**. Compound (*S*)-**8k** occupied the binding site in an extended form. In this orientation, the pyrano[3,2-*c*]quinoline and benzyl moieties of compound (*S*)-**8k** filled the bottom and the entrance of the active site, respectively (Figure 4). (*S*)-**8k** established interactions with the key residues including Gly70, Phe158, Gln181, Asp214, Glu276, Glu304, Arg312, His348, and Asp349. The benzyl group of compound (*S*)-**8k** formed a π-anion interaction with the carboxylate moiety of Glu304 and a π-alkyl interaction with the side chain of Arg312. The importance of the 1,2,3-triazole ring in proper orientation of these derivatives in the active site of α-glucosidase was determined by forming two hydrogen bonds with key residue Arg312. In addition, the 1,2,3-triazole ring formed a π-anion interaction with residue Asp349. Furthermore, the central phenoxy group made a T-shaped $\pi-\pi$ interaction with residue Phe158. In addition, quinolone created a π-anion interaction with Glu276 and $\pi-\pi$ stacking interaction with His348. Moreover, the two hydrogen bonds were seen between the carbonyl group and nitrogen atom of

https://doi.org/10.1021/acsomega.3c00133
ACS Omega 2023, 8, 23412−23424

Table 2. Results of the Ensemble Docking of Acarbose, 8e, 8g, and 8k into the Active Site of the α-Glucosidase Enzyme in 6 Models Obtained from Clustering of the MD Simulation Trajectories[a]

compound		ΔH	$-T\Delta S$	ΔG_b	95% CI	$\sum q^2$	μ	Q
acarbose		−13.56	1.79	−11.77	[−10.53, −6.69]	2.65	6.93	27.17
8e	*R*	−13.12	1.79	−11.33	[−10.49, −10.19]	1.06	5.94	8.99
	S	−13.38	1.79	−11.59	[−10.66, −10.28]	1.06	5.95	8.99
8g	*R*	−12.47	1.79	−10.68	[−10.15, −9.82]	1.18	2.82	24.37
	S	−13.56	1.79	−11.77	[−10.87, −10.26]	1.18	2.82	24.37
8k	*R*	−11.99	2.09	−9.90	[−10.48, −10.10]	1.64	2.43	23.92
	S	−13.05	2.09	−10.96	[−10.57, −10.37]	1.64	2.43	23.92

[a]Mulliken charges, dipole moment (μ), and quadrupole moment (Q) were calculated using the semiempirical method AM1. 95% CI of the estimated free energy of binding was calculated by 10^6 cycles of the bootstrapping method. ΔH: final intermolecular energy, $-T\Delta S$: ∼torsional free energy, and ΔG_b: estimated free energy of binding (all in kcal/mol)

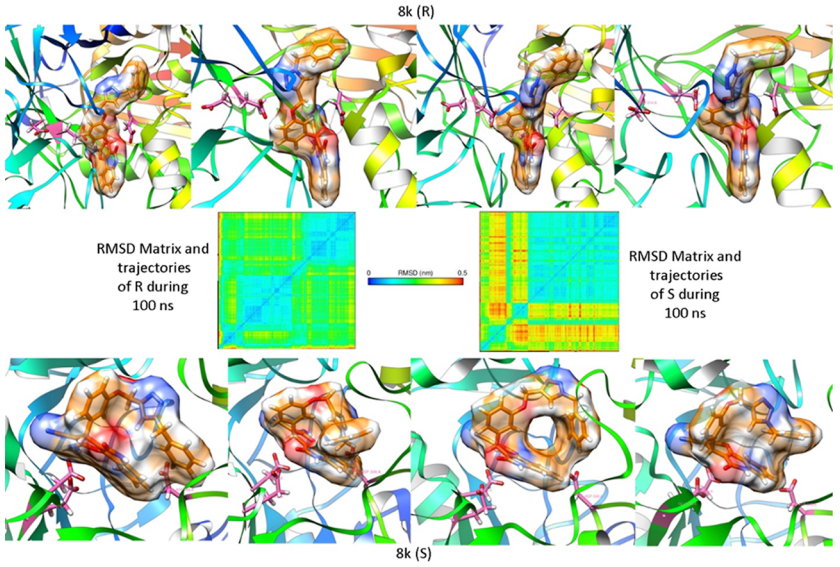

Figure 5. rmsd matrix and trajectories of compound **8k** (*R*- and *S*-enantiomers) during the 100 ns MD simulations. The catalytic triad residues Asp214, Glu276, and Asp349 is shown by pink sticks. (*S*)-**8k** experienced more conformational variations in the active site of the α-glucosidase enzyme in comparison to the R-enantiomer. (*R*)-**8k** seemed to be stable in the whole MD simulation time, but the *S*-enantiomer started to drift back out of the active site. Notice the distance between the **8k** and the triad amino acids.

the quinolone moiety and the residues Gln181 and Asp214, respectively.

Compound (*R*)-**8k** established interactions with the key residues including Phe177, Thr215, His239, Asn241, Glu276, His279, Ser308, Arg312, and Asp348 (Figure 4). The binding mode of the *R*-enantiomer was inverse to the *S*-enantiomer. The benzyl group of (*R*)-**8k** was placed in the bottom of the active site and formed vdW interactions with Glu276 as one of the catalytic triad residues. The pyrano[3,2-*c*]quinoline moiety was directed to the entrance of the enzyme active site and interacted with residues His279 and His239 via $\pi-\pi$ interactions and the 1,2,3-triazol ring formed vdW and T-shaped $\pi-\pi$ interactions with residues Thr215, Asp349, and Phe177, respectively. Furthermore, the CN, NH_2, and carbonyl groups of pyrano[3,2-*c*]quinoline moiety made three hydrogen bonds with residues Arg312, Ser308, and Asn241. Also, the central phenoxy group established a π-cation interaction with Arg312.

The interaction profile of compound **8k** showed that most functional groups interacted with the α-glucosidase active site and had an efficient contribution in free energy of binding. Due to the importance of explicit water and the flexibility of the receptor in the binding process, a 100 ns MD simulation was performed on the predicted complexes in the docking approach.

2.2.5. Molecular Dynamics Simulation. 100 ns MD simulations were performed in the best ensemble docking models to get more realistic compound **8k** (*R*- and *S*-enantiomers)-α-glucosidase complexes. The stability of the simulated systems was checked by monitoring total energy and temperature during the 100 ns production run. These thermodynamic parameters converged to an equilibrium state in less than 1 ns from the start of the MD simulation. The average temperature in 100 ns of the MD simulation at 300 K was equal to 300.6 K (±1.3 and 1.2) for *S*- and *R*-enantiomers of compound **8g** in complex with α-glucosidase. The total energy of the systems was steady during the MD simulation (rsd <0.18%). So, the results indicated that energy conservation was satisfied in the simulations process.

rmsd of the α-glucosidase backbone atoms reached a plateau after 19 ns in both systems (average rmsd of the backbone is 0.30 ± 0.060 nm—rsd <19.6% in the *R*-enantiomer and 0.25 ± 0.021 nm—rsd <8.3% in the *S*-enantiomer). The radius of gyration was constant during the whole MD run (rsd <0.23 and 0.59% in *R*- and *S*-enantiomers, respectively).

The stability of both enantiomers in the active site of α-glucosidase was evaluated using the rmsd matrix (Figure 5).

https://doi.org/10.1021/acsomega.3c00133
ACS Omega 2023, 8, 23412−23424

Figure 5 illustrates that compound (*R*)-**8k** formed a stable complex in the active site of the enzyme during the 100 ns MD simulation (blue square in the rmsd matrix indicates fluctuation less than 0.15 nm). In the initial steps of the MD simulation, a meta stable state could be tracked (red regions in the rmsd matrix of (*R*)-**8k** that finally reach a stable state). In this regard, the ligand passed through a transition state (big blue square) and remained stable in this conformer. These conformational changes caused the (*R*)-compound **8k** enantiomer to drift deeper into the active site of the α-glucosidase enzyme. On the other hand, the (*S*)-compound **8k** enantiomer drifted back out from the active site during the MD simulation time (notice the red and yellow regions in the rmsd matrix and conformational changes during the MD simulation time).

Interaction profiles of the *R*- and *S*-enantiomer of compound **8k** revealed that the *R*-enantiomer was bound to α-glucosidase more effectively. The electrostatic interactions between the two enantiomers and α-glucosidase is inclined toward the *R*-enantiomer (−60.6 ± 4.3 kcal/mol in comparison to −18.6 ± 5.9 kcal/mol in (*S*)-**8k**). Contribution of the vdW interactions was more than that of the electrostatic interactions in binding energy. The vdW interactions of (*R*)-**8k** were −53.0 ± 2.8 kcal/mol. The stability and binding energy for both enantiomers indicated that the *R*-enantiomer (binding energy: −73.6 ± 3.8 kcal/mol) had higher binding affinity to the active site of the enzyme rather than the *S*-enantiomer (binding energy: −62.4 ± 5.9 kcal/mol). The in silico results were in accordance with the experimental data that related the potency to the substitution on the benzyl ring. The benzyl ring in the most stable complex ((*R*)-compound **8k**) was located in the binding site and interacted with the enzyme active site more than the pyrano[3,2-*c*]quinoline moiety that occupied high solvent accessible entrance of the active site.

3. CONCLUSIONS

The findings of the present study indicated that all of the synthesized pyrano[3,2-*c*]quinoline-1,2,3-triazole hybrids **8a**−**o** significantly inhibited the α-glucosidase activity of *S. cerevisiae*. Compound **8k** was found to be the most active agent against this enzyme in a competitive manner with an IC_{50} value of 1.19 ± 0.05. In silico study revealed that both *R*- and *S*-enantiomers of compound **8k** interacted with critical amino acids in the enzyme active site. However, the *R*-enantiomer exhibited more stability and binding affinity to the active site of the α-glucosidase enzyme rather than the *S*-enantiomer. The hydrophobic benzyl moiety of the *R*-enantiomer showed a tendency to occupy the bottom of the enzyme active site, while the hydrophilic pyrano[3,2-*c*]-quinoline moiety interacted with the active site entrance. Thus, the synthesized pyrano[3,2-*c*]quinoline-1,2,3-triazole hybrids seem to be promising scaffolds for the development of novel α-glucosidase inhibitors.

4. EXPERIMENTAL SECTION

Melting points were measured on a Kofler hot stage apparatus and are uncorrected. The NMR (^{1}H and ^{13}C) and IR spectra were obtained by using a Bruker 400-, 300-NMR, and α FT-IR spectrometer on KBr discs, respectively. Elemental analysis was performed on an Elementar Analysen GmbH VarioEL CHNS mode. MS spectra were recorded by an Agilent Technology (HP) mass spectrometer operating at an ionization potential of 70 eV. All chemicals were obtained from Merck and Aldrich.

4.1. Chemistry. *4.1.1. General Procedure for the Synthesis of 4-(Prop-2-yn-1-yloxy)benzaldehyde Derivatives (**3a**−**c**).* In a 25 mL round-bottomed flask, 1 mmol of benzaldehyde derivatives (**1a**−**c**), 1.2 mmol of propargyl bromide 80%, and 1.5 mmol of potassium carbonate in DMF (5 mL) were stirred at room temperature for 24 h. The reaction solution was poured into crushed ice, and then the solid precipitate was filtered and washed with water. The (**3a**−**c**) derivatives were used for the next step without further purification.[35]

*4.1.2. General Procedure for the Synthesis of 2-Amino-5-oxo-4-(4-(prop-2-yn-1-yloxy)phenyl)-5,6-dihydro-4H-pyrano[3,2-c]quinoline-3-carbonitrile (**6a**−**c**).* In a 25 mL round-bottomed flask, 1 mmol of derivatives **3a**−**c**, 1.2 mmol of malononitrile, and 4-hydroxyquinoline-2 (1*H*)-one (1 mmol) in ethanol 98% (5 mL) were stirred for 4 h under reflux conditions. After the reaction was completed, the precipitated product was filtered and washed with ethanol. The **6a**−**c** derivatives were used for the next step without further purification.[36]

*4.1.3. General Procedure for the Synthesis of 2-Amino-4-(4-((1-benzyl-1H-1,2,3-triazol-4-yl)methoxy)phenyl)-5-oxo-5,6-dihydro-4H-pyrano[3,2-c]quinoline-3-carbonitrile (**8a**−**o**).* To generate the benzyl azide derivatives, NaN_3 (1.5 mmol) and various benzyl halide derivatives (1.2 mmol) were stirred in DMF (4 mL) at room temperature for 2 h. Intermediates **6a**−**c**, 2 drops of NEt_3, ascorbic acid (5% mmol), $CuSO_4{\cdot}5H_2O$ (5%mmol), and H_2O (1 mL) were added to the previous solution and stirred at room temperature for 24 h to obtain final quinoline-1,2,3-triazole hybrids **8a**−**o**. After completion of the reaction, ice was added to the reaction mixture and the resulting precipitate (**8a**−**o**) was filtered and washed with water.[17]

*4.1.3.1. 2-Amino-4-(4-((1-benzyl-1H-1,2,3-triazol-4-yl)-methoxy)phenyl)-5-oxo-5,6-dihydro-4H-pyrano[3,2-c]-quinoline-3-carbonitrile (**8a**).* White solid; yield: 59%, mp 168−171 °C. FT-IR (KBr) ν_{max} (cm^{-1}): 3324, 3188, 2961, 2868, 2197, 1672, 1507, 1381, 1257, 1174, 762; ^{1}H NMR (300 MHz, DMSO-d_6): δ_{ppm} 11.79 (s, 1H, NH), 8.29 (s, 1H, H-triazole), 7.92 (d, J = 7.5 Hz, 1H, H_{10}), 7.60 (t, J = 7.5 Hz, 1H, H_9), 7.26−7.40 (m, 9H, NH_2, H_7, H_8, $H_{2''}$, $H_{3''}$, $H_{4''}$, $H_{5''}$, $H_{6''}$), 7.13 (d, J = 8.6 Hz, 2H, $H_{2'}$, $H_{6'}$), 6.95 (d, J = 8.6 Hz, 2H, $H_{3'}$, $H_{5'}$), 5.62 (s, 2H, CH_2−O), 5.10 (s, 2H, CH_2), 4.46 (s, 1H, H_4), ^{13}C NMR (76 MHz, DMSO-d_6): δ_{ppm} 160.98, 159.44, 157.35, 151.45, 138.15, 137.28, 136.44, 133.55, 131.68, 129.23, 128.94, 128.68, 128.63, 128.42, 125.19, 122.28, 120.38, 115.81, 114.98, 112.51, 110.32, 61.53, 58.43, 53.33, 36.33. Anal. Calcd for $C_{29}H_{22}N_6O_3$: C, 69.31; H, 4.41; N, 16.72. Found: C, 69.62; H, 4.35; N, 16.50.

*4.1.3.2. 2-Amino-4-(4-((1-(4-methylbenzyl)-1H-1,2,3-triazol-4-yl)methoxy)phenyl)-5-oxo-5,6-dihydro-4H-pyrano[3,2-c]quinoline-3-carbonitrile (**8b**).* White solid; yield: 40%, mp 146−148 °C. IR (KBr): FT-IR (KBr) ν_{max} (cm^{-1}): 3457, 3327, 2925, 2863, 2197, 1671, 1648, 1509, 1381, 1257, 1129, 1107, 764; ^{1}H NMR (300 MHz, DMSO-d_6): δ_{ppm} 11.79 (s, 1H, NH), 8.25 (s, 1H, H-triazole), 7.92 (d, J = 8.1 Hz, 1H, H_{10}), 7.59 (t, J = 8.1 Hz, 1H, H_9), 7.35 (d, J = 8.1 Hz, 1H, H_7), 7.19−7.31 (m, 7H, NH_2, H_8, $H_{2''}$, $H_{3''}$ $H_{5''}$, $H_{6''}$), 7.15 (d, J = 8.8 Hz, 2H, $H_{2'}$, $H_{6'}$), 6.95 (d, J = 8.8 Hz, 2H, $H_{3'}$, $H_{5'}$), 5.55 (s, 2H, CH_2−O), 5.09 (s, 2H, CH_2), 4.47 (s, 1H, H_4), 2.28 (s, 3H, $-CH_3$). ^{13}C NMR (76 MHz, DMSO-d_6): δ_{ppm} 160.96,

https://doi.org/10.1021/acsomega.3c00133
ACS Omega 2023, 8, 23412−23424

159.42, 157.37, 151.43, 138.20, 137.98, 137.29, 133.47, 131.63, 129.76, 128.97, 128.51, 124.92, 122.45, 122.24, 120.42, 115.82, 114.94, 112.52, 110.33, 61.55, 58.39, 53.12, 36.37, 21.17. Anal. Calcd for $C_{30}H_{24}N_6O_3$: C, 69.76; H, 4.68; N, 16.27. Found: C, 69.42; H, 4.55; N, 16.10.

*4.1.3.3. 2-Amino-4-(4-((1-(4-fluorobenzyl)-1H-1,2,3-triazol-4-yl)methoxy)phenyl)-5-oxo-5,6-dihydro-4H-pyrano[3,2-c]quinoline-3-carbonitrile (**8c**).* White solid; yield: 61%, mp 192−194 °C. IR (KBr) ν_{max} (cm^{-1}): 3404, 3327, 2925, 2863, 2197, 1671, 1648, 1622, 1509, 1381, 1257, 1129, 1115, 1107, 764; ^{1}H NMR (300 MHz, DMSO-d_6): δ_{ppm} 11.79 (s, 1H, NH), 8.30 (s, 1H, H-triazole), 7.92 (d, J = 8.1 Hz, 1H, H_{10}), 7.59 (t, J = 8.1 Hz, 1H, H_9), 7.19−7.44 (m, 8H, NH_2, H_7, H_8, $H_{2''}$, $H_{3''}$, $H_{5''}$, $H_{6''}$), 7.14 (d, J = 8.5 Hz, 2H, $H_{2'}$, $H_{6'}$), 6.95 (d, J = 8.5 Hz, 2H, $H_{3'}$, $H_{5'}$), 5.61 (s, 2H, CH_2−O), 5.01 (s, 2H, CH_2), 4.47 (s, 1H, H_4). ^{13}C NMR (76 MHz, DMSO-d_6): δ_{ppm} 163.96, 160.96, 160.73, 159.41, 157.36, 151.43, 138.20, 137.31, 132.76, 132.71, 131.64, 130.87, 130.75, 128.98, 125.03, 122.46, 122.24, 120.42, 116.23, 115.95, 115.81, 114.94, 112.51, 110.32, 61.54, 58.38, 52.50, 36.37. MS: m/z (%) = 520.2 (M^+, 1), 361.1 (2), 287.0 (2), 213.0 (3), 133.1 (4), 98 (52), 80 (100). Anal. Calcd for $C_{29}H_{21}FN_6O_3$: C, 66.92; H, 4.07; N, 16.15. Found: C, 66.81; H, 4.15; N, 16.20.

*4.1.3.4. 2-Amino-4-(4-((1-(4-chlorobenzyl)-1H-1,2,3-triazol-4-yl)methoxy)phenyl)-5-oxo-5,6-dihydro-4H-pyrano[3,2-c]quinoline-3-carbonitrile (**8d**).* White solid; yield: 57%, mp 140−142 °C. ^{1}H NMR (300 MHz, DMSO-d_6): δ_{ppm} 11.78 (s, 1H, NH), 8.30 (s, 1H, H-triazole), 7.92 (d, J = 7.2 Hz, 1H, H_{10}), 7.59 (t, J = 7.2 Hz, 1H, H_9), 7.26−7.47 (m, 8H, NH_2, H_7, H_8, $H_{2''}$, $H_{3''}$, $H_{5''}$, $H_{6''}$), 7.14 (d, J = 8.3 Hz, 2H, $H_{2'}$, $H_{6'}$), 6.95 (d, J = 8.3 Hz, 2H, $H_{3'}$, $H_{5'}$), 5.62 (s, 2H, CH_2−O), 5.11 (s, 2H, CH_2), 4.47 (s, 1H, H_4). ^{13}C NMR (76 MHz, DMSO-d_6): δ_{ppm} 160.95, 159.42, 157.36, 151.43, 138.20, 137.32, 135.47, 133.36, 131.64, 130.42, 129.25, 128.98, 125.19, 122.45, 122.23, 115.82, 114.95, 112.52, 110.33, 61.55, 58.39, 52.50, 36.37. Anal. Calcd for $C_{29}H_{21}ClN_6O_3$: C, 64.87; H, 3.94; N, 15.65. Found: C, 65.71; H, 4.10; N: 15.41.

*4.1.3.5. 2-Amino-4-(4-((1-(4-bromobenzyl)-1H-1,2,3-triazol-4-yl)methoxy)phenyl)-5-oxo-5,6-dihydro-4H-pyrano[3,2-c]quinoline-3-carbonitrile (**8e**).* White solid; yield:51%, mp 203−205 °C. ^{1}H NMR (300 MHz, DMSO-d_6): δ_{ppm} 11.79 (s, 1H, NH), 8.30 (s, 1H, H-triazole), 7.92 (d, J = 8.1 Hz, 1H, H_{10}), 7.57−7.61 (m, 3H, H_9, $H_{5''}$, $H_{3''}$), 7.27−7.36 (m, 6H, NH_2, H_7, H_8, $H_{2''}$, $H_{6''}$), 7.14 (d, J = 8.7 Hz, 2H, $H_{2'}$, $H_{6'}$), 6.96 (d, J = 8.7 Hz, 2H, $H_{3'}$, $H_{5'}$), 5.61 (s, 2H, CH_2−O), 5.11 (s, 2H, CH_2), 4.47 (s, 1H, H_4). ^{13}C NMR (76 MHz, DMSO-d_6): δ_{ppm} 160.95, 159.41, 157.36, 151.43, 138.20, 137.32, 135.89, 132.18, 131.64, 130.73, 128.98, 122.45, 122.23, 121.92, 115.82, 114.94, , 112.51, 110.32, 61.54, 58.38, 52.56, 36.37. MS: m/z (%) = 583.1 (M + 2^+, 1), 581.1.1 (M^+, 1), 279.0 (2), 238.0 (3), 213 (4), 149 (7), 133.1 (4), 98 (52), 80 (100). Anal. Calcd for $C_{29}H_{21}BrN_6O_3$: C, 59.91; H, 3.64; N, 14.45. Found: C, 60.11; H, 3.59; N: 14.48.

*4.1.3.6. 2-Amino-4-(4-((1-benzyl-1H-1,2,3-triazol-4-yl)-methoxy)-3-methoxyphenyl)-5-oxo-5,6-dihydro-4H-pyrano-[3,2-c]quinoline-3-carbonitrile (**8f**).* White solid; yield: 83%, mp 185−186 °C. IR (KBr) ν_{max} (cm^{-1}): 3325, 3179, 3003, 2867, 2194, 1673, 1629, 1559, 1378, 1029, 755; ^{1}H NMR (400 MHz, DMSO-d_6): δ_{ppm} 11.78 (s, 1H, NH), 8.26 (s, 1H, H-triazole), 7.91 (d, J = 6.5 Hz, 1H, H_{10}), 7.58 (t, J = 6.5 Hz, 1H, H_9), 7.28−7.38 (m, 7 H, H_7, H_8, $H_{2''}$, $H_{3''}$, $H_{4''}$, $H_{5''}$, $H_{6''}$), 7.25 (s, 2H−NH_2), 7.03 (d, J = 8.3 Hz, 1H, $H_{5'}$), 6.87 (s, 1H, $H_{2'}$), 6.56 (d, J = 8.3 Hz, 1H, $H_{6'}$), 5.60 (s, 2H, CH_2−O), 5.06 (s, 2H, CH_2), 4.47 (s, 1H, H_4), 3.69 (s, 3H, −OMe), ^{13}C NMR (100 MHz, DMSO-d_6): δ_{ppm} 160.51, 159.03, 151.01, 148.68, 146.31, 137.70, 137.50, 135.98, 131.14, 131.09, 128.72, 128.10, 127.92, 124.74, 121.94, 121.74, 119.02, 115.31, 113.74, 112.02, 111.73, 109.72, 61.76, 57.71, 55.41, 52.78, 36.13. MS: m/z (%) = 532.2 (M^+, 1), 279.0 (2), 212.9 (4), 133.1 (4), 98 (50), 79.9 (100). Anal. Calcd for $C_{30}H_{24}N_6O_4$: C, 67.66; H, 4.54; N, 15.78. Found: C, 67.79; H, 4.49; N, 15.82.

*4.1.3.7. 2-Amino-4-(3-methoxy-4-((1-(4-methylbenzyl)-1H-1,2,3-triazol-4-yl)methoxy)phenyl)-5-oxo-5,6-dihydro-4H-pyrano[3,2-c]quinoline-3-carbonitrile (**8g**).* White solid; yield: 85%, mp 164−168 °C. IR (KBr) ν_{max} (cm^{-1}): 3438, 2924, 2866, 1674, 1628, 1588, 1512, 1379, 1269, 1136, 1031, 759; ^{1}H NMR (300 MHz, DMSO-d_6): δ_{ppm} 11.80 (s, 1H, NH), 8.24 (s, 1H, H-triazole), 7.92 (d, J = 7.7 Hz, 1H, H_{10}), 7.59 (t, J = 7.7 Hz, 1H, H_9), 7.17−7.37 (m, 8H, NH_2, H_7, H_8, $H_{2''}$, $H_{3''}$ $H_{5''}$, $H_{6''}$), 7.03 (d, J = 8.2 Hz, 1H, $H_{5'}$), 6.88 (s, 1H, s, 1H, $H_{2'}$), 6.67 (d, J = 8.2 Hz, 1H, $H_{6'}$), 5.55 (s, 2H, CH_2−O), 5.06 (s, 2H, CH_2), 4.49 (s, 1H, H_4), 3.89 (s, 3H, −OMe), 2.28 (s, 3H, −Me), ^{13}C NMR (76 MHz, DMSO-d_6): δ_{ppm} 161.03, 159.53, 151.52, 149.16, 146.83, 138.21, 137.99, 133.45, 131.66, 129.80, 129.76, 128.59, 128.53, 122.45, 122.25, 119.54, 115.82, 114.17, 112.53, 112.19, 110.21, 62.26, 58.21, 55.90, 53.12, 36.64, 21.18. MS: m/z (%) = 546.2 (M^+, 1), 279.0 (2), 167.1 (25), 125.1 (100), 89 (12). Anal. Calcd for $C_{31}H_{26}N_6O_4$: C, 68.12; H, 4.79; N, 15.38. Found: C, 68.19; H, 4.69; N, 15.58.

*4.1.3.8. 2-Amino-4-(4-((1-(4-fluorobenzyl)-1H-1,2,3-triazol-4-yl)methoxy)-3-methoxyphenyl)-5-oxo-5,6-dihydro-4H-pyrano[3,2-c]quinoline-3-carbonitrile (**8h**).* White solid; yield: 88%, mp 146−148 °C. ^{1}H NMR (400 MHz, DMSO-d_6): δ_{ppm} 11.86 (s, 1H, NH), 8.33 (s, 1H, H-triazole), 7.98 (d, J = 7.8 Hz, 1H, H_{10}), 7.66 (t, J = 7.8, 1H, H_9), 7.28−7.48 (m, 8H, NH_2, H_7, H_8, $H_{2''}$, $H_{3''}$, $H_{5''}$, $H_{6''}$), 7.11 (d, J = 8.0 Hz, 1H, $H_{5'}$), 6.95 (s, 1H, s, 1H, $H_{2'}$), 7.43 (d, J = 8.0 Hz, 1H, $H_{6'}$), 5.67 (s, 2H, CH_2−O), 5.13 (s, 2H, CH_2), 4.55 (s, 1H, H_4), 3.76 (s, 3H, −OMe), ^{13}C NMR (100 MHz, DMSO-d_6): δ_{ppm} 163.06, 160.61, 160.52, 159.00, 151.01, 148.63, 146.30, 137.69, 137.50, 132.22, 132.20, 131.15, 130.36, 130.28, 124.62, 121.95, 121.74, 119.03, 115.68, 115.47, 115.30, 113.63, 112.01, 111.65, 109.68, 61.71, 57.69, 55.38, 51.97, 36.13. MS: m/z (%) = 550.2 (M^+, 1), 336.1 (2), 279.1 (7), 149.1 (45), 80 (13), 73 (100). Anal. Calcd for $C_{30}H_{23}FN_6O_4$: C, 65.5; H, 4.21; N, 15.27. Found: C, 65.33; H, 4.25; N, 15.46.

*4.1.3.9. 2-Amino-4-(4-((1-(4-chlorobenzyl)-1H-1,2,3-triazol-4-yl)methoxy)-3-methoxyphenyl)-5-oxo-5,6-dihydro-4H-pyrano[3,2-c]quinoline-3-carbonitrile (**8i**).* White solid; yield: 69%, mp174−176 °C. IR (KBr): 3333, 3179, 2929, 2854, 2193, 1674, 1628, 1597, 1511, 1378, 1269, 1137, 1016, 763; ^{1}H NMR (300 MHz, DMSO-d_6): δ_{ppm} 11.80 (s, 1H, NH), 8.30 (s, 1H, H-triazole), 7.92 (d, J = 7.6 Hz, 1H, H_{10}), 7.59 (t, J = 7.6 Hz, 1H, H_9), 7.27−7.50 (m, 8H, NH_2, H_7, H_8, $H_{2''}$, $H_{3''}$, $H_{5''}$, $H_{6''}$), 7.04 (d, J = 8.2, 1H, $H_{5'}$), 6.89 (s, 1H, $H_{2'}$), 6.67 (d, J = 8.2 Hz, 1H, $H_{6'}$), 5.62 (s, 2H, CH_2−O), 5.07 (s, 2H, CH_2), 4.49 (s, 1H, H_4), 3.70 (s, 3H, −OMe), ^{13}C NMR (76 MHz, DMSO-d_6): δ_{ppm} 161.03, 159.54, 151.54, 149.19, 146.83, 138.21, 138.06, 135.42, 133.38, 131.65, 130.78, 130.50, 130.45, 129.25, 129.18, 122.45, 122.26, 119.57, 115.83, 114.24, 112.53, 112.24, 110.20, 62.28, 58.22, 55.92, 52.53, 36.65. Anal. Calcd for $C_{30}H_{23}ClN_6O_4$: C, 63.55; H, 4.09; N, 14.82. Found: C, 63.43; H, 4.15; N: 14.96.

*4.1.3.10. 2-Amino-4-(4-((1-(4-bromobenzyl)-1H-1,2,3-triazol-4-yl)methoxy)-3-methoxyphenyl)-5-oxo-5,6-dihydro-4H-pyrano[3,2-c]quinoline-3-carbonitrile (**8j**).* White solid; yield:

https://doi.org/10.1021/acsomega.3c00133
ACS Omega 2023, 8, 23412−23424

64%, mp 180−183 °C. ^{1}H NMR (400 MHz, DMSO-d_6): δ_{ppm} 11.78 (s, 1H, NH), 8.27 (s, 1H, H-triazole), 7.90 (d, J = 8.0 Hz, 1H, H_{10}), 7.57−7.60 (m, 3H, H_9, $H_{3''}$, $H_{5''}$), 7.25−7.35 (m, 6 H, NH_2, H_7, H_8, $H_{2''}$, $H_{6''}$), 7.03 (d, J = 8.2 Hz, 1H, $H_{5'}$), 6.87 (s, 1H, s, 1H, $H_{2'}$), 6.66 (d, J = 8.2 Hz, 1H, $H_{6'}$), 5.59 (s, 2H, CH_2−O), 5.06 (s, 2H, CH_2), 4.47 (s, 1H, H_4), 3.69 (s, 3H, −OMe), ^{13}C NMR (100 MHz, DMSO-d_6): δ_{ppm} 160.51, 159.01, 151.01, 148.66, 146.32, 137.69, 137.52., 135.37, 131.66, 131.15, 130.23, 124.82, 121.94, 121.75, 121.41, 119.05, 115.31, 113.68, 112.01, 111.69, 109.69, 61.75, 57.70, 55.40, 52.03, 36.13. Anal. Calcd for $C_{30}H_{23}BrN_6O_4$: C, 58.93; H, 3.79; N, 13.74. Found: C, 59.13; H, 3.85; N, 13.89.

*4.1.3.11. 2-Amino-4-(3-((1-benzyl-1H-1,2,3-triazol-4-yl)-methoxy)phenyl)-5-oxo-5,6-dihydro-4H-pyrano[3,2-c]-quinoline-3-carbonitrile (**8k**).* White solid; yield: 63%, mp 203−233 °C. IR (KBr): 3191, 3151, 2923, 2861, 2189, 1671, 1550, 1384, 1258, 1106, 1026, 763; ^{1}H NMR (400 MHz, DMSO-d_6): δ_{ppm} 11.88 (s, 1H, NH), 8.39 (s, 1H, H-triazole), 8.00 (d, J = 8.2 Hz, 1H, H_{10}), 7.67 (t, J = 8.2 Hz,1H, H_9), 7.37−7.46 (m, 9 H, NH_2, H_7, H_8, $H_{1''}$, $H_{2''}$, $H_{3''}$, $H_{5''}$, $H_{6''}$), 7.31 (t, J = 8.0 Hz, 1H, $H_{5'}$), 7.01 (d, J = 8.0 Hz, 1H, $H_{4'}$), 6.92 (s, 1H, $H_{2'}$), 6.88 (d, J = 8.0 Hz, 1H, $H_{6'}$), 5.68 (s, 2H, CH_2−O), 5.19 (s, 2H, CH_2), 4.59 (s, 1H, H_4), ^{13}C NMR (100 MHz, DMSO-d_6): δ_{ppm} 160.45, 159.00, 157.94, 151.25, 146.01, 137.75, 135.95, 131.20, 129.54, 128.72, 128.09, 127.93, 124.78, 121.95, 121.76, 119.88, 119.81, 115.34, 114.44, 112.19, 111.98, 109.39, 60.99, 57.57, 52.81, 36.56. MS: m/z (%) = 502.2 (M^+, 1), 336.1 (2), 288.1 (5), 91.1 (30), 64 (100). Anal. Calcd for $C_{29}H_{22}N_6O_3$: C, 69.31; H, 4.41; N, 16.72. Found: C, 69.42; H, 4.57; N, 16.66.

*4.1.3.12. 2-Amino-4-(3-((1-(4-methylbenzyl)-1H-1,2,3-triazol-4-yl)methoxy)phenyl)-5-oxo-5,6-dihydro-4H-pyrano[3,2-c]quinoline-3-carbonitrile (**8l**).* White solid; yield: 40%, mp 222−226 °C. IR (KBr): 3371, 3176, 2921, 2862, 2196, 1679, 1591, 1490, 1415, 1376, 1257, 1162, 1009, 768; ^{1}H NMR (300 MHz, DMSO-d_6): δ_{ppm} 11.79 (s, 1H, NH), 8.27 (s, 1H, H-triazole), 7.92 (d, J = 7.0 Hz, 1H, H_{10}), 7.60 (t, J = 7.0 Hz, 1H, H_9), 7.19−7.37 (m, 9 H, 2H−NH_2, H_7, H_{10}, H_5, $H_{2''}$, $H_{3''}$ $H_{5''}$ $H_{6''}$), 6.93 (d, J = 8.4 Hz, 1H, $H_{4'}$), 6.79−6.84 (m, 2H, $H_{2'}$, $H_{6'}$), 5.54 (s, 2H, CH_2−O), 5.10 (s, 2H, CH_2), 4.50 (s, 1H, H_4), 2.29 (s, 3H, −Me). ^{13}C NMR (76 MHz, DMSO-d_6): δ_{ppm} 160.96, 159.52, 158.45, 151.75, 146.51, 143.36, 138.27, 137.95, 133.46, 131.71, 130.05, 129.76, 128.48, 125.06, 122.47, 122.27, 120.37, 115.85, 114.95, 112.72, 112.49, 109.91, 61.49, 58.08, 53.12, 37.07, 21.17. Anal. Calcd for $C_{30}H_{24}N_6O_3$: C, 69.76; H, 4.68; N, 16.27. Found: C, 69.62; H, 4.57; N, 16.16.

*4.1.3.13. 2-Amino-4-(3-((1-(4-fluorobenzyl)-1H-1,2,3-triazol-4-yl)methoxy)phenyl)-5-oxo-5,6-dihydro-4H-pyrano[3,2-c]quinoline-3-carbonitrile (**8m**).* White solid; yield: 55%, mp 228−231 °C. IR (KBr): 3325, 3190, 2926, 2862, 2191, 1673, 1602, 1552, 1511, 1411, 1382, 1268, 1167, 1021, 762; ^{1}H NMR (400 MHz, DMSO-d_6): δ_{ppm} 11.87 (s, 1H, NH), 8.39 (s, 1H, H-triazole), 8.00 (d, J = 8.2 Hz, 1H, H_{10}), 7.67 (t, J = 8.2 Hz, 1H, H_9), 7.27−7.50 (m, 9 H, H_8, H_7, NH_2, $H_{5'}$, $H_{2''}$, $H_{3''}$, $H_{5''}$, $H_{6''}$), 7.01 (d, J = 8.0 Hz, 1H, $H_{4'}$), 6.92 (s, 1H, $H_{2'}$), 6.89 (d, J = 8.0 Hz, 1H, $H_{6'}$), 5.68 (s, 2H, CH_2−O), 5.18 (s, 2H, CH_2), 4.58 (s, 1H, H_4). ^{13}C NMR (100 MHz, DMSO-d_6): δ_{ppm} 163.06, 160.45, 159.00, 157.92, 151.24, 146.01, 142.93, 137.75, 132.21, 132.19, 131.20, 130.31, 130.23, 129.54, 129.44, 124.63, 121.95, 121.76, 119.88, 119.80, 115.67, 115.45, 115.34, 114.45, 112.19, 111.97, 109.38, 60.98, 57.56, 51.99, 36.55. Anal. Calcd for $C_{29}H_{21}FN_6O_3$: C, 66.92; H, 4.07; N, 16.15. Found: C, 66.51; H, 4.17; N, 16.13.

*4.1.3.14. 2-Amino-4-(3-((1-(4-chlorobenzyl)-1H-1,2,3-triazol-4-yl)methoxy)phenyl)-5-oxo-5,6-dihydro-4H-pyrano[3,2-c]quinoline-3-carbonitrile (**8n**).* White solid; yield: 56%, mp 213−216 °C. ^{1}H NMR (300 MHz, DMSO-d_6): δ_{ppm} 11.82 (s, 1H, NH), 8.33 (s, 1H, H-triazole), 7.94 (d, J = 7.9 Hz, 1H, H_{10}), 7.59 (t, J = 7.9 Hz 1H, H_9), 7.25−7.45 (m, 9 H, H_7, H_8, NH_2, $H_{5'}$, $H_{2''}$, $H_{3''}$, $H_{5''}$, $H_{6''}$), 6.94 (d, J = 8.0 Hz, 1H, $H_{4'}$), 6.88 (s, 1H, $H_{2'}$), 6.84 (d, J = 8.0 Hz, 1H, $H_{6'}$), 5.62 (s, 2H, CH_2−O), 5.13 (s, 2H, CH_2), 4.54 (s, 1H, H_4). ^{13}C NMR (76 MHz, DMSO-d_6): δ_{ppm} 161.01, 159.53, 158.45, 151.79, 146.55, 143.49, 138.27, 135.40, 133.37, 131.69, 130.36, 130.07, 129.22, 125.28, 122.46, 122.28, 120.44, 120.37, 115.86, 115.01, 112.72, 112.51, 109.90, 61.50, 58.15, 52.53, 37.10. Anal. Calcd for $C_{29}H_{21}ClN_6O_3$: C, 64.87; H, 3.94; N, 15.65. Found: C, 64.73; H, 4.05; N, 15.54.

*4.1.3.15. 2-Amino-4-(3-((1-(4-bromobenzyl)-1H-1,2,3-triazol-4-yl)methoxy)phenyl)-5-oxo-5,6-dihydro-4H-pyrano[3,2-c]quinoline-3-carbonitrile (**8o**).* White solid; yield: 43%, mp 153−155 °C. ^{1}H NMR (300 MHz, DMSO-d_6): δ_{ppm} 11.81 (s, 1H, NH), 8.33 (s, 1H, H-triazole), 7.93 (d, J = 9.0 Hz, 1H, H_{10}), 7.56−7.61 (m, 3H, H_9, $H_{2''}$, $H_{6''}$), 7.25−7.35 (m, 7 H, 2H−NH_2, H_7, H_8, $H_{5'}$, $H_{3''}$, $H_{5''}$), 6.94 (d, J = 8.0 Hz, 1H, $H_{4'}$), 6.86 (s, 1H, $H_{2'}$) −6.87 (d, J = 8.0 Hz, 1H, $H_{6'}$), 5.60 (s, 2H, CH_2−O), 5.12 (s, 2H, CH_2), 4.53 (s, 1H, H_4). ^{13}C NMR (76 MHz, DMSO-d_6): δ_{ppm} 160.99, 159.52, 158.44, 151.78, 146.54, 143.48, 138.27, 135.84, 132.16, 131.70, 130.67, 130.06, 125.30, 122.46, 122.28, 121.91, 120.42, 120.36, 119.90, 115.86, 115.00, 112.71, 112.50, 109.90, 61.49, 58.11, 52.58, 37.09. MS: m/z (%) = 583.2 ($M+2^+$, 1), 581.2 (M^+, 1), 369.1 (2), 279.1 (5), 238.1 (7), 149.0 (60), 80 (100). Anal. Calcd for $C_{29}H_{21}BrN_6O_3$: C, 59.91; H, 3.64; N, 14.42. Found: C, 59.98; H, 3.81; N, 14.38.

4.2. *In Vitro* α-Glucosidase Inhibition Assay. The α-Glucosidase enzyme (from *S. cerevisiae*, EC3.2.1.20, 20 U/mg) and the substrate (*p*-nitrophenyl glucopyranoside) were purchased from Sigma-Aldrich. An appropriate concentration of the enzyme was prepared in potassium phosphate buffer (pH 6.8, 50 mM), and 4,5-diarylimidazole-1,2,3-triazole hybrids **8a**−**o** were dissolved in DMSO (final concentration 10%). The enzyme (20 μL), different concentrations of the synthesized compounds (20 μL), and potassium phosphate buffer (135 μL) were added to a 96-well plate and incubated at 37 °C for 10 min. Then, the substrate (25 μL, 4 mM) was added to each well of the plate and incubated at 37 °C for 20 min. Finally, the change in the absorbance was measured at 405 nm by using a Gen5 spectrophotometer (Power wave xs2, BioTek, America). DMSO, as a solvent control, and acarbose, as the standard inhibitor drug, were used. The percentage of inhibition for the synthesized compounds **8a**−**o**, the control, and acarbose was calculated by using the following formula

$$\% \text{ inhibition} = [(\text{Abs control} - \text{Abs sample})/\text{Abs control}] \times 100$$

The IC_{50} values of the tested agents were determined from the nonlinear regression curve using the logit method.[37]

4.3. Kinetic Study. The α-glucosidase solution (1 U/mL, 20 μL) was incubated with different concentrations of compound **8k** (0, 0.5, 1.25, and 2.5 μM) at 30 °C for 15 min. The enzymatic reaction was initiated by adding various concentrations of *p*-nitrophenyl glucopyranoside as the substrate substance (1−10 mM). Then, change in the absorbance was measured for 20 min at 405 nm by using a

https://doi.org/10.1021/acsomega.3c00133
ACS Omega 2023, 8, 23412−23424

spectrophotometer (Gen5, Power wave xs2, BioTek, America).[37]

4.4. Homology Modeling. The sequence of the eukaryotic yeast *S. cerevisiae* α-glucosidase was retrieved from the NCBI database (accession number P53341). The BLAST module in the NCBI was utilized to search the best template with the known structures in the Protein Data Bank.[34] According to the obtained results, the isomaltase enzyme from the baker's yeast (accession number P53051, PDB ID: 3A4A) at 1.60 Å resolution was selected as a template for the homology modeling study. A pairwise sequence alignment was generated using CLUSTALW based on the default parameters.[38] Following the sequence alignment, the structure of the isomaltase enzyme was used as a template for building an α-glucosidase model with the Modeller 9v24 software.[39] A number of 10^6 conformations of α-glucosidase was generated. The best model was selected with the lowest value of the DOPE. The general stereochemical quality of the final selected model was evaluated using the Ramachandran plot provided by PROCHECK.[40]

4.5. Docking Study. The 3D structures of acarbose and the selected compounds **8e**, **8g**, and **8k** were optimized by ORCA using the PBE0/def2-TZVP method.[41] AM1BCC charges and torsional degree of freedom were assigned for each ligand. Polar hydrogen atoms and Koullman charges were added to the enzyme structure using AutoDockTools-1.5.4. AutoGrid maps for each atom type in the ligands, were calculated with 0.375 Å spacing between grid points. The center of the grid box was placed at $x = 85.87$, $y = 69.585$, and $z = 40.072$. The dimensions of the active site box were set at 60 × 60 × 60 Å. Flexible ligand dockings were accomplished for the selected compounds. 200 GA runs, 27,000 maximum generations, a gene mutation rate of 0.02, and a crossover rate of 0.8 were set for the LGA method. The lowest energy conformation of the highest populated cluster was selected for the analysis. Graphic visualizations were done by Chimera software.

4.6. MD Simulation. The MD simulation was performed using the GROMACS-2019 package with a standard AMBER99SB-ILDN force field. Ligand atom types were assigned by using ANTECHAMBER. Partial atomic charges were calculated using the AM1BCC method. The predicted complex of the α-glucosidase enzyme and the selected compounds was centered in a dodecahedron box and solvated in water molecules represented by the TIP3P model. Sixteen water molecules were replaced with nine Na^+ atoms to get electro-neutrality. Linear constraint solver was used to constrain all bonds to their initial length. The particle mesh Ewald method with a cutoff length of 14 Å and cubic interpolation was used for both long range electrostatic and van der Waals interactions. Energy minimization was carried out using 10,000 cycles of steepest descent. The system was heated to 300 K in 100 ps and was equilibrated in *NVT* and *NPT* ensembles in each 100 ps. For production run, all of the constraints were removed and the 100 ns MD simulation was carried out in the *NPT* ensemble.

■ ASSOCIATED CONTENT

Supporting Information

The Supporting Information is available free of charge at https://pubs.acs.org/doi/10.1021/acsomega.3c00133.

Spectral data for all compounds (FT-IR, NMR, and mass spectra) (PDF)

■ AUTHOR INFORMATION

Corresponding Author

Zahra Najafi − *Department of Medicinal Chemistry, School of Pharmacy, Hamadan University of Medical Sciences, Hamadan 6517838678, Iran;* orcid.org/0000-0001-8189-1586; Phone: +988138381676; Email: najafi.zch@gmail.com, z.najafi@umsha.ac.ir; Fax: +9881 38381591

Authors

Soheila Esmaili − *Department of Organic Chemistry, Faculty of Chemistry, Bu-Ali Sina University, Hamedan 6517838683, Iran*

Ahmad Ebadi − *Department of Medicinal Chemistry, School of Pharmacy, Medicinal Plants and Natural Products Research Center, Hamadan University of Medical Sciences, Hamadan 6517838678, Iran*

Ardeshir Khazaei − *Department of Organic Chemistry, Faculty of Chemistry, Bu-Ali Sina University, Hamedan 6517838683, Iran*

Hamideh Ghorbani − *Department of Medicinal Chemistry, School of Pharmacy, Hamadan University of Medical Sciences, Hamadan 6517838678, Iran*

Mohammad Ali Faramarzi − *Department of Pharmaceutical Biotechnology, Faculty of Pharmacy and Biotechnology Research Center, Tehran University of Medical Sciences, Tehran 1417614411, Iran;* orcid.org/0000-0002-8822-453X

Somayeh Mojtabavi − *Department of Pharmaceutical Biotechnology, Faculty of Pharmacy and Biotechnology Research Center, Tehran University of Medical Sciences, Tehran 1417614411, Iran*

Mohammad Mahdavi − *Endocrinology and Metabolism Research Center, Endocrinology and Metabolism Clinical Sciences Institute, Tehran University of Medical Sciences, Tehran 1416753955, Iran*

Complete contact information is available at: https://pubs.acs.org/10.1021/acsomega.3c00133

Author Contributions

S.E. synthesized and analyzed all of the compounds. A.E. and H.G. performed the molecular dynamics study. M.F. and S.M. performed *in vitro* α-glucosidase study. A.K. and M.M. provided some starting materials. Z.N. designed and edited the manuscript. All authors contributed to the subsequent revision of the manuscript.

Notes

The authors declare no competing financial interest.

■ ACKNOWLEDGMENTS

This work was supported by Vice-chancellor for Research and Technology of Hamadan University of Medical Sciences with project no. 140106084786.

■ REFERENCES

(1) Deng, Y.; Li, N.; Wu, Y.; Wang, M.; Yang, S.; Zheng, Y.; Deng, X.; Xiang, D.; Zhu, Y.; Xu, P.; Zhai, Z.; Zhang, D.; Dai, Z.; Gao, J. Global, Regional, and National Burden of Diabetes-Related Chronic Kidney Disease From 1990 to 2019. *Front. Endocrinol.* **2021**, *12*, 672350.

(2) León-Jiménez, D.; Miramontes-González, J. P.; Márquez-López, L.; Astudillo-Martín, F.; Beltrán-Romero, L. M.; Moreno-Obregón, F.; Escalada-San Martín, J. Basal insulin analogues in people with diabetes and chronic kidney disease. *Diabetic Med.* **2022**, *39*, No. e14679.
(3) Andreadi, A.; Bellia, A.; Di Daniele, N.; Meloni, M.; Lauro, R.; Della-Morte, D.; Lauro, D. The molecular link between oxidative stress, insulin resistance, and type 2 diabetes: A target for new therapies against cardiovascular diseases. *Curr. Opin. Pharmacol.* **2022**, *62*, 85−96.
(4) Bradley, P. Hypothesis: Enhanced glucose availability and insulin resistance enhances an activated immune system and accounts for the obesity paradox. *Clin. Obes.* **2022**, *12*, No. e12521.
(5) Fadem, S. Z. *Staying Healthy with Kidney Disease*; Springer, 2022.
(6) Lin, C.-F.; Liu, H.-C.; Lin, S.-Y. Kidney Function and Risk of Physical and Cognitive Impairment in Older Persons with Type 2 Diabetes at an Outpatient Clinic with Geriatric Assessment Implementation. *Diabetes, Metab. Syndr. Obes.: Targets Ther.* **2022**, *15*, 79−91.
(7) Escandón-Rivera, S.; González-Andrade, M.; Bye, R.; Linares, E.; Navarrete, A. s.; Mata, R. α-Glucosidase Inhibitors from Brickellia cavanillesii. *J. Nat. Prod.* **2012**, *75*, 968−974.
(8) Shen, X.; Saburi, W.; Gai, Z.; Kato, K.; Ojima-Kato, T.; Yu, J.; Komoda, K.; Kido, Y.; Matsui, H.; Mori, H.; et al. Structural analysis of the α-glucosidase HaG provides new insights into substrate specificity and catalytic mechanism. *Acta Crystallogr., Sect. D: Biol. Crystallogr.* **2015**, *71*, 1382−1391.
(9) Hossain, U.; Das, A. K.; Ghosh, S.; Sil, P. C. An overview on the role of bioactive α-glucosidase inhibitors in ameliorating diabetic complications. *Food Chem. Toxicol.* **2020**, *145*, 111738.
(10) Leonhardt, W.; Hanefeld, M.; Fischer, S.; Schulze, J. Efficacy of α-glucosidase inhibitors on lipids in NIDDM subjects with moderate hyperlipidaemia. *Eur. J. Clin. Invest.* **1994**, *24*, 45−49.
(11) Chapel, C.; Garcia, C.; Roingeard, P.; Zitzmann, N.; Dubuisson, J.; Dwek, R. A.; Trepo, C.; Zoulim, F.; Durantel, D. Antiviral effect of α-glucosidase inhibitors on viral morphogenesis and binding properties of hepatitis C virus-like particles. *J. Gen. Virol.* **2006**, *87*, 861−871.
(12) Tundis, R.; Loizzo, M.; Menichini, F. Natural products as α-amylase and α-glucosidase inhibitors and their hypoglycaemic potential in the treatment of diabetes: an update. *Mini-Rev. Med. Chem.* **2010**, *10*, 315−331.
(13) Mahmood, N. A review of α-amylase inhibitors on weight loss and glycemic control in pathological state such as obesity and diabetes. *Comp. Clin. Pathol.* **2016**, *25*, 1253−1264.
(14) Najafi, Z.; Mahdavi, M.; Saeedi, M.; Karimpour-Razkenari, E.; Asatouri, R.; Vafadarnejad, F.; Moghadam, F. H.; Khanavi, M.; Sharifzadeh, M.; Akbarzadeh, T. Novel tacrine-1, 2, 3-triazole hybrids: In vitro, in vivo biological evaluation and docking study of cholinesterase inhibitors. *Eur. J. Med. Chem.* **2017**, *125*, 1200−1212.
(15) Najafi, Z.; Mahdavi, M.; Saeedi, M.; Karimpour-Razkenari, E.; Edraki, N.; Sharifzadeh, M.; Khanavi, M.; Akbarzadeh, T. Novel tacrine-coumarin hybrids linked to 1, 2, 3-triazole as anti-Alzheimer's compounds: In vitro and in vivo biological evaluation and docking study. *Bioorg. Chem.* **2019**, *83*, 303−316.
(16) Karypidou, K.; Ribone, S. R.; Quevedo, M. A.; Persoons, L.; Pannecouque, C.; Helsen, C.; Claessens, F.; Dehaen, W. Synthesis, biological evaluation and molecular modeling of a novel series of fused 1,2,3-triazoles as potential anti-coronavirus agents. *Bioorg. Med. Chem. Lett.* **2018**, *28*, 3472−3476.
(17) Tian, Y.; Liu, Z.; Liu, J.; Huang, B.; Kang, D.; Zhang, H.; De Clercq, E.; Daelemans, D.; Pannecouque, C.; Lee, K.-H.; et al. Targeting the entrance channel of NNIBP: Discovery of diarylnicotinamide 1, 4-disubstituted 1, 2, 3-triazoles as novel HIV-1 NNRTIs with high potency against wild-type and E138K mutant virus. *Eur. J. Med. Chem.* **2018**, *151*, 339−350.
(18) Son Hai, D.; Thi Thu Ha, N.; Tien Tung, D.; Thi Kim Giang, N.; Thi Thu Huong, N.; Huu Anh, H.; Thi Kim Van, H.; Ngoc Toan, V.; Toan, D. N.; Thanh, N. D. Synthesis, biological evaluation and induced fit docking simulation study of d-glucose-conjugated 1 H-1, 2, 3-triazoles having 4 H-pyrano [2, 3-d] pyrimidine ring as potential agents against bacteria and fungi. *New J. Chem.* **2022**, *46*, 8303−8323.
(19) Bangalore, P. K.; Vagolu, S. K.; Bollikanda, R. K.; Veeragoni, D. K.; Choudante, P. C.; Misra, S.; Sriram, D.; Sridhar, B.; Kantevari, S. Usnic acid enaminone-coupled 1, 2, 3-triazoles as antibacterial and antitubercular agents. *J. Nat. Prod.* **2019**, *83*, 26−35.
(20) Srinivas Reddy, M.; Swamy Thirukovela, N.; Narsimha, S.; Ravinder, M.; Kumar Nukala, S. Synthesis of fused 1, 2, 3-triazoles of Clioquinol via sequential CuAAC and CH arylation; in vitro anticancer activity, in silico DNA topoisomerase II inhibitory activity and ADMET. *J. Mol. Struct.* **2022**, *1250*, 131747.
(21) Singh, H.; Singh, J. V.; Gupta, M. K.; Saxena, A. K.; Sharma, S.; Nepali, K.; Bedi, P. M. S. Triazole tethered isatin-coumarin based molecular hybrids as novel antitubulin agents: Design, synthesis, biological investigation and docking studies. *Bioorg. Med. Chem. Lett.* **2017**, *27*, 3974−3979.
(22) Singh, H.; Kumar, M.; Nepali, K.; Gupta, M. K.; Saxena, A. K.; Sharma, S.; Bedi, P. M. S. Triazole tethered C5-curcuminoid-coumarin based molecular hybrids as novel antitubulin agents: Design, synthesis, biological investigation and docking studies. *Eur. J. Med. Chem.* **2016**, *116*, 102−115.
(23) Sharma, S.; Gupta, M. K.; Saxena, A. K.; Bedi, P. M. S. Triazole linked mono carbonyl curcumin-isatin bifunctional hybrids as novel anti tubulin agents: Design, synthesis, biological evaluation and molecular modeling studies. *Bioorg. Med. Chem.* **2015**, *23*, 7165−7180.
(24) Singh, J.; Sharma, S.; Saxena, A. K.; Nepali, K.; Bedi, P. M. S. Synthesis of 1, 2, 3-triazole tethered bifunctional hybrids by click chemistry and their cytotoxic studies. *Med. Chem. Res.* **2013**, *22*, 3160−3169.
(25) Wang, G.; Peng, Z.; Wang, J.; Li, X.; Li, J. Synthesis, in vitro evaluation and molecular docking studies of novel triazine-triazole derivatives as potential α-glucosidase inhibitors. *Eur. J. Med. Chem.* **2017**, *125*, 423−429.
(26) Avula, S. K.; Khan, A.; Rehman, N. U.; Anwar, M. U.; Al-Abri, Z.; Wadood, A.; Riaz, M.; Csuk, R.; Al-Harrasi, A. Synthesis of 1H-1,2,3-triazole derivatives as new α-glucosidase inhibitors and their molecular docking studies. *Bioorg. Chem.* **2018**, *81*, 98−106.
(27) Asgari, M. S.; Mohammadi-Khanaposhtani, M.; Kiani, M.; Ranjbar, P. R.; Zabihi, E.; Pourbagher, R.; Rahimi, R.; Faramarzi, M. A.; Biglar, M.; Larijani, B.; et al. Biscoumarin-1,2,3-triazole hybrids as novel anti-diabetic agents: Design, synthesis, in vitro α-glucosidase inhibition, kinetic, and docking studies. *Bioorg. Chem.* **2019**, *92*, 103206.
(28) Mohammadi-Khanaposhtani, M.; Rezaei, S.; Khalifeh, R.; Imanparast, S.; Faramarzi, M. A.; Bahadorikhalili, S.; Safavi, M.; Bandarian, F.; Nasli Esfahani, E.; Mahdavi, M.; et al. Design, synthesis, docking study, α-glucosidase inhibition, and cytotoxic activities of acridine linked to thioacetamides as novel agents in treatment of type 2 diabetes. *Bioorg. Chem.* **2018**, *80*, 288−295.
(29) Taha, M.; Ismail, N. H.; Imran, S.; Wadood, A.; Rahim, F.; Ali, M.; Rehman, A. U. Novel quinoline derivatives as potent in vitro α-glucosidase inhibitors: in silico studies and SAR predictions. *MedChemComm* **2015**, *6*, 1826−1836.
(30) Lee, H.-W.; Yang, J.-Y.; Lee, H.-S. Quinoline-2-carboxylic acid isolated from Ephedra pachyclada and its structural derivatives show inhibitory effects against α-glucosidase and α-amylase. *J. Korean Soc. Appl. Biol. Chem.* **2014**, *57*, 441−444.
(31) Chehardoli, G.; Gholamhoseini, P.; Ebadi, A.; Ziaei, M.; Akbarzadeh, T.; Saeedi, M.; Mahdavi, M.; Khoshneviszadeh, M.; Najafi, Z. 6-Methoxy-1-tetralone Derivatives Bearing an N-Arylpyridinium Moiety as Cholinesterase Inhibitors: Design, Synthesis, Biological Evaluation, and Molecular Docking Study. *ChemistrySelect* **2022**, *7*, No. e202201977.
(32) Sadafi Kohnehshahri, M.; Chehardoli, G.; Bahiraei, M.; Akbarzadeh, T.; Ranjbar, A.; Rastegari, A.; Najafi, Z. Novel tacrine-based acetylcholinesterase inhibitors as potential agents for the treatment of Alzheimer's disease: Quinolotacrine hybrids. *Mol. Diversity* **2022**, *26*, 489−503.

https://doi.org/10.1021/acsomega.3c00133
ACS Omega 2023, 8, 23412−23424

(33) Liu, M.; Zhang, W.; Qiu, L.; Lin, X. Synthesis of butyl-isobutyl-phthalate and its interaction with -glucosidase in vitro. *J. Biochem.* **2011**, *149*, 27−33.
(34) Altschul, S. F.; Gish, W.; Miller, W.; Myers, E. W.; Lipman, D. J. Basic local alignment search tool. *J. Mol. Biol.* **1990**, *215*, 403−410.
(35) Somakala, K.; Amir, M.; Sharma, V.; Wakode, S. Synthesis and pharmacological evaluation of pyrazole derivatives containing sulfonamide moiety. *Monatsh. fur Chem.* **2016**, *147*, 2017−2029.
(36) Lei, M.; Ma, L.; Hu, L. A green, efficient, and rapid procedure for the synthesis of 2-amino-3-cyano-1, 4, 5, 6-tetrahydropyrano [3, 2-c] quinolin-5-one derivatives catalyzed by ammonium acetate. *Tetrahedron Lett.* **2011**, *52*, 2597−2600.
(37) Adib, M.; Peytam, F.; Rahmanian-Jazi, M.; Mahernia, S.; Bijanzadeh, H. R.; Jahani, M.; Mohammadi-Khanaposhtani, M.; Imanparast, S.; Faramarzi, M. A.; Mahdavi, M.; et al. New 6-amino-pyrido[2,3-d]pyrimidine-2,4-diones as novel agents to treat type 2 diabetes: A simple and efficient synthesis, α-glucosidase inhibition, molecular modeling and kinetic study. *Eur. J. Med. Chem.* **2018**, *155*, 353−363.
(38) Thompson, J. D.; Higgins, D. G.; Gibson, T. J. CLUSTAL W: improving the sensitivity of progressive multiple sequence alignment through sequence weighting, position-specific gap penalties and weight matrix choice. *Nucleic Acids Res.* **1994**, *22*, 4673−4680.
(39) Šali, A.; Blundell, T. L. Comparative protein modelling by satisfaction of spatial restraints. *J. Mol. Biol.* **1993**, *234*, 779−815.
(40) Laskowski, R. A.; MacArthur, M. W.; Moss, D. S.; Thornton, J. M. PROCHECK: a program to check the stereochemical quality of protein structures. *J. Appl. Crystallogr.* **1993**, *26*, 283−291.
(41) Neese, F.; Wennmohs, F.; Becker, U.; Riplinger, C. The ORCA quantum chemistry program package. *J. Chem. Phys.* **2020**, *152*, 224108.

https://doi.org/10.1021/acsomega.3c00133
ACS Omega 2023, 8, 23412−23424